Journal of Catalysis 281 (2011) 300–308

Contents lists available at ScienceDirect

Journal of Catalysis

journal homepage: www.elsevier.com/locate/jcat

A quantitative investigation of the structure of Raney-Ni catalyst material using both computer simulation and experimental measurements

N.C. Barnard [a], S.G.R. Brown [a,*], F. Devred [b], J.W. Bakker [b], B.E. Nieuwenhuys [b], N.J. Adkins [c]

[a] Materials Research Centre, College of Engineering, Swansea University, Singleton Park, Swansea SA2 8PP, United Kingdom
[b] Leiden Institute of Chemistry, Leiden University, Einsteinweg 55, 2333 CC Leiden, The Netherlands
[c] IRC in Materials Processing, The University of Birmingham, Edgbaston, Birmingham B15 2TT, United Kingdom

ARTICLE INFO

Article history:
Received 12 November 2010
Revised 7 May 2011
Accepted 10 May 2011
Available online 15 June 2011

Keywords:
Monte Carlo simulation
Raney-nickel catalysts
Spray-atomisation

ABSTRACT

This paper describes combined experimental techniques and numerical modelling of the surface condition of activated nanoscopic Raney-nickel catalysts produced via leaching of spray-atomised NiAl precursor powders. Results of off-lattice Metropolis and lattice kinetic Monte Carlo models compare favourably to experimentation quantifying the surface of Raney-nickel catalysts in terms of both surface area and the surface distribution of residual aluminium left over from the leaching process. Predicted surface areas from the kinetic Monte Carlo simulations are shown to be in good agreement with BET measurements from nitrogen physisorption for catalyst materials prepared from two different NiAl precursor alloys. Surface aluminium concentrations predicted by Metropolis Monte Carlo simulations are also in agreement with X-ray photoelectron spectroscopy results and in addition predict an absence of Al–Al bonding at the surface.

1. Introduction

Raney-type nickel catalysts are prepared by removing aluminium from a Ni–Al alloy using a sodium hydroxide solution [1–3]. This activation process is of crucial importance for the structure and properties of Raney-type nickel catalysts. However, the structure and composition of the starting alloy also play an important role in the performance of the final catalyst [4–8]. To our knowledge, combined numerical modelling and experimental measurements concerning the leaching process for Raney-type nickel catalysts has not been reported earlier.

In this paper, two separate Monte Carlo models are used and compared to experimental measurement. The first, a lattice kinetic Monte Carlo model, attempts to predict the nano-porous structure of the so-called 'spongy' nickel produced during leaching of Ni–Al alloy. The second, an off-lattice Metropolis Monte Carlo model, uses this predicted structure to attempt to describe the likely nature of the surface of the Raney-Ni catalyst in terms of surface segregation of residual Al atoms. In order to correlate the model with experimental data, bulk analysis (inductively coupled plasma optical emissions spectroscopy) and surface analysis (X-ray photoelectron spectroscopy and BET) were performed on catalysts prepared from spray-atomised starting alloy. The surface of the catalyst (where the catalytic reactions occur) is of particular interest. Holm and Storp, in 1976, were the first to use XPS for the characterisation of the surface of both starting alloys and the resulting Raney-type catalysts [8]. Since then published XPS data have provided conflicting results. These discrepancies could be caused by differences in experimental procedures or in the interpretation of the results, yet the most likely explanation is the variation of starting alloys used by different research groups. A major point of discussion is the chemical state of the Ni and Al at the catalyst surface. It has been claimed that Ni and Al are in the metallic state in activated catalysts [9–14]. However, it has also been reported that next to metallic Ni, oxidic Ni is present in activated catalysts. In the latter, aluminium is generally claimed to be in an ionic state at the surface [15–20].

In this study, simulation of the leaching process is presented using a combination of kinetic Monte Carlo [21] and Metropolis Monte Carlo [22] methods with periodic boundary conditions. In parallel, X-ray photoelectron spectroscopy, bulk analysis and BET measurements are performed to correlate simulation results with experimental data.

2. Numerical models

In this section, the details of the numerical models used and their controlling parameters are described. First, the kinetic Monte Carlo (kMC) method is covered with reference to its use of Arrhenius relationships, attempt frequencies used, interatomic potentials, the time-stepping algorithm and finally the activation energies arising from the model. The advantages and limitations of the kMC approach then serve to introduce the Metropolis Monte

* Corresponding author. Fax: +44 (0)1792 295676.
E-mail address: s.g.r.brown@swansea.ac.uk (S.G.R. Brown).

0021-9517/$ - see front matter © 2011 Elsevier Inc. All rights reserved.
doi:10.1016/j.jcat.2011.05.010

Carlo (MMC) model. General descriptions of these two techniques are widely available in the literature, e.g., [21,22].

2.1. Kinetic Monte Carlo method

In order to simulate the time evolution of the leaching of a Raney-Ni structure, a kinetic Monte Carlo method is used [23,24]. The model is based on work by Erlebacher et al. [25] who used this technique to model the leaching of silver from a Au–50 at.% (atomic percent) Ag alloy, examining the evolution of nano-porosity. For NiAl alloys, two key processes are assumed to be taking place during leaching, namely adatom diffusion (Ni or Al) and Al dissolution. These processes are assumed to occur at known rates that serve as the inputs for the model. For both diffusion and dissolution, a bond breaking model is used. The activation barrier that an atom with coordination number n must exceed to either diffuse or dissolve is the sum of the bond energies of all of its neighbouring atoms, nE_b, and both diffusion and dissolution of adatoms are assumed to proceed at a rate described by the following Arrhenius relationships, respectively:

$$k_n^{diff} = \upsilon_{diff} \exp\left(-\frac{nE_b}{k_B T}\right) \quad (1)$$

$$k_n^{diss} = \upsilon_{diss} \exp\left(-\frac{nE_b}{k_B T}\right) \quad (2)$$

where k_n^{diff} is the rate constant for diffusion of an adatom (Ni or Al), k_n^{diss} is the rate constant for dissolution of an adatom (Al only), υ_{diff} and υ_{diss} are the frequency factors for adatom diffusion and Al dissolution respectively, n is the number of bonds, k_B is the Boltzmann constant, T is absolute temperature (K). The pre-exponential factors for these processes are expected to be about 10^{13} s^{-1}. For all leaching simulations, a constant temperature of 353 K is used to match the experimental leaching temperature and simulations are run for 180 min to match the experimental procedure.

The potential barrier for dissolution is located near the surface, the rate of dissolution depends on the potential, and this dependence is expected to be described by the conventional Butler–Volmer equation [26]. Here, we include the potential-related factor into the pre-exponential factor, and with this modification, the pre-exponential factor becomes apparent and may be appreciably higher than 10^{13} s^{-1}. As the accurate value of the transfer coefficient in the Butler–Volmer equation is lacking, we simply postulate that the apparent potential factor is 10^{17} s^{-1} based on numerical results described below.

2.2. Attempt frequencies and the kMC model

In the spirit of a combined modelling/experimental paper, a pragmatic approach has been taken to determine the value of υ_{diss} used in the model. Since this kMC model is confined to a fixed computational lattice, it does not simulate the grain boundaries/lattice defects. Also the effects of any reaction products are not included. In reality, polycrystalline structures are present and some authors have also proposed a fragmentation mechanism of such a structure during leaching [27]. In order to choose a value for υ_{diss}, with which to obtain realistic kinetics of dissolution, published measurements of the rate of removal of Al from precursor material as a function of time are used. The vertical bars in Fig. 1 show measured Al content after 10 s and 300 s of leaching for two different commercial 50–50 Ni/Al wt.% alloys [28], i.e., corresponding to a Ni–Al 68.5 at.% alloy. It can be seen from Fig. 1 that removal of Al via leaching has effectively finished after 10 s. Fig. 1 shows the predicted removal rates of Al for $NiAl_3$ and Ni_2Al_3 phases, simulated separately, for values of υ_{diss} of 10^{16}, 10^{17} and 10^{18} s^{-1}. First of all, it can be seen from this figure that the effect of the choice of υ_{diss} on the

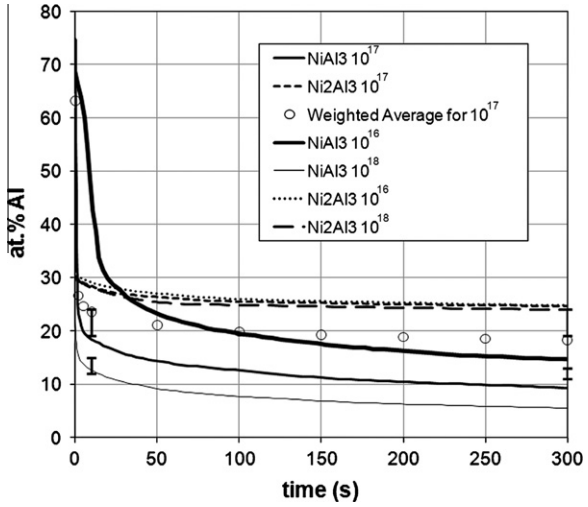

Fig. 1. Loss of aluminium during the first 300 s of leaching for dissolution attempt frequencies of 10^{16}, 10^{17} and 10^{18} s^{-1} for $NiAl_3$ and Ni_2Al_3 simulations, where the diffusion attempt frequency is constant at 10^{13} s^{-1} in all cases. The vertical bars at 10 s and 300 s are experimental measurements taken from Ref. [26]. The circles represent a volume fraction weighted average for the 10^{17} s^{-1} case.

leaching of Ni_2Al_3 phase is very small. Assuming typical proportions of $NiAl_3$, Ni_2Al_3 and Al phases of 33, 62 and 5% respectively [29] and assuming all of the Al phase dissolves immediately, a volume fraction weighted average can be calculated for the amount of Al in the material as a function of time. It can be seen that choosing a value of $\upsilon_{diss} = 10^{17}$ s^{-1} the weighted average percentage of Al is a good match to the experimental measurements.

Although dissolution of Al occurs very quickly in practice, the leaching procedure is carried out for 3 h to ensure removal of reaction products. During this time, coarsening of the structure occurs via atomic diffusion. Fig. 2 shows the effect of the value of υ_{diss} on the coarsening of the structure for $NiAl_3$ phase. A very steep initial rise in surface area followed by a slower decrease with time is predicted. From this figure, it can be seen that although there are initial differences in the very early stages, the final predicted surface area of the leached material is relatively insensitive to υ_{diss} and the same effect is found to be true for the Ni_2Al_3 phase. In contrast, it

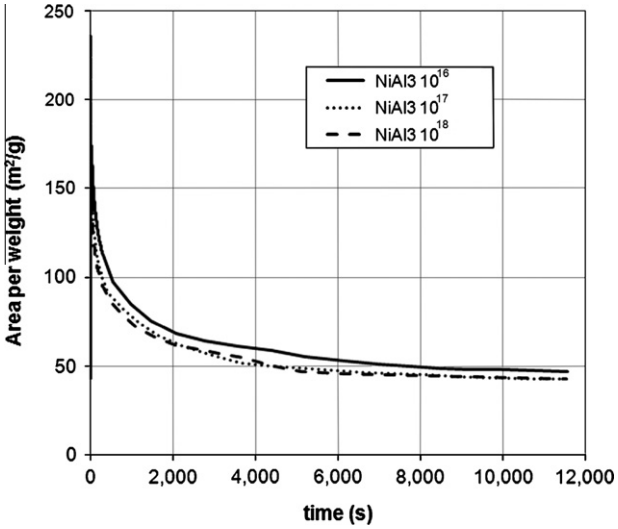

Fig. 2. Predicted area per weight evolution over time for the full leaching process (3 h) for dissolution attempt frequencies of 10^{16}, 10^{17} and 10^{18} s^{-1} for $NiAl_3$, where the diffusion attempt frequency is constant at 10^{13} s^{-1} in all cases.

would be expected that the time-dependent coarsening of the structure is much more dependent on v_{diff} and this is found to be the case in simulations. In this work, a value of v_{diff} of the order of the Debye frequency is used because it has previously been used very successfully in surface-diffusion driven simulations of morphological evolution, e.g., [30–32]. Although these latter references concern behaviour in ultra high vacuum more recent studies investigate other environments [33–37].

2.3. Interatomic potentials and the kMC model

The atomistic model potentials used, E_b, are based on the work carried out in [38], which involved a mathematical transformation between atomic volume and a local variable function. In this work, potential parameters were determined by fitting energy surfaces resulting from full-potential linear combination of muffin-tin orbitals (LMTO) total-energy calculations to density functional theory (DFT) calculations. The interatomic potentials used were calculated via:

$$E_b = E(\omega)/N - \frac{1}{2}\sum_{i\neq j}^{nn} \psi_{s_i s_j}(r_{ij}) \tag{3}$$

where ω is the atomic volume, N is the total number of atoms, s_i is the reference lattice system and r_{ij} is the interatomic distance. The form given in [38] for the first term in Eq. (3) is used, in addition to the parameterized form for the pair interactions, ψ, using $\psi_0 = -0.330$, -0.375 and -0.138 eV for Ni–Ni, Ni–Al and Al–Al bonds, respectively. Atomistic potentials were calculated over the number of nearest neighbour atoms, nn [39], and in the present model, it is assumed that the crystal is without any type of lattice defect, and the role of any reaction products is not included. Within the current model, vacancy formation and surface relaxation are not considered, and it is acknowledged that a more sophisticated model of atomic bonding could be of benefit, e.g., effective-medium theory [40], embedded atom method [41] or Finnis–Sinclair (F–S) type many-body potentials [42]. However, experimental data with which to compare more complicated models, especially in the early, vigorously agitated stages of leaching, are not currently available. In situ leaching experimentation carried out at the ILL (Institut Laue-Langevin, Grenoble, France) by other workers associated with the current project has been carried out to provide further detail on the precise leaching processes occurring in these materials [G.N. Iles, F. Devred, U. Dahlborg, G. Reinhart, M. Calvo-Dahlborg, B.E. Nieuwenhuys, In situ studies of the leaching process in Al–Ni alloys, ILL Experimental Report 5-25-156, January 2009, ILL: D20 – high intensity powder diffraction]. However, the data are yet to be analysed in more detail and will be published in the near future.

The surface diffusion of both elements during leaching means that the final nanoscopic spongy nickel structure is not 'revealed' but 'constructed' during leaching by diffusion of Ni adatoms. Eqs. (1) and (2a) ensure that atoms with fewer bonds are more likely to dissolve or diffuse. Adatoms either already present in, or diffusing to, lower energy sites (i.e., sites of higher coordination number) will tend to become less likely to diffuse further. In this way, Ni adatoms tend to cluster together at surfaces that are increasingly exposed during Al dissolution, thus building up a nanoscopic structure.

2.4. Time stepping and the BKL algorithm in the kMC model

Knowledge of the rates of all permitted transitions allows the time increment for any iteration of the model to be calculated. This has been done using the well-known Bortz–Kalos–Lebowitz (BKL) algorithm to determine the evolution of the spongy nickel on an event-by-event basis. For completeness, a brief description of the algorithm is provided here.

1. Set elapsed time to zero; $t = 0$.
2. Determine all possible transition states and calculate the cumulative function, $R_i = \sum_{j=1}^{i} k_j$ for $i = 1, \ldots, N$, total number of transitions. The total number of transitions is all possible adatom diffusion/dissolution events.
3. Get a uniform random number, $u \in (0, 1]$.
4. Find the event to carry out, i, for which $R_{i-1} < uR < R_j$.
5. Find all transitions and associated rates, k_i that have changed due to the transition.
6. Get another random number, $u \in (0, 1]$.
7. Update the time with $t = t + \Delta T$, where $\Delta T = -\log(u)/R$.
8. Return to step 2.

In this paper model results for leaching of the $NiAl_3$ phase are presented. To carry out a simulation, a 3D computational domain is created containing Ni and Al atoms in atomic proportions 1:3 in an $AuCu_3$ structure (a computationally convenient approximation of the $NiAl_3$ structure [43]). Initially a cubic region of material is created, all faces of which are considered to be exposed to concentrated NaOH solution. The BKL algorithm is then applied with the result that Al atoms are progressively removed (at a rate that decreases with time). Simultaneously, adatom diffusion of Ni results leads to the development of a nano-porous structure.

2.5. Activation energies and the kMC model

Before proceeding further, the activation energies associated with dissolution and diffusion events are considered. In transition state theory terms, the diffusion rates of Ni and Al atoms and the dissolution rates of Al atoms will depend on lateral interactions in the activated and ground states [44], and these rates are expected to vary according to different arrangements of atoms. It should be noted that the rates of diffusion and dissolution depend on the metal–metal interactions in the ground and activated states and that these interactions for these processes are very different.

In a real system, the jump rates associated with diffusion/dissolution events will be widely distributed whereas in the kMC model this distribution is much smaller. In order to evaluate the parameters used in the model, we now focus on the particular activation energies dominating diffusion/dissolution events in the model. In the BKL algorithm, all possible adatom diffusion/dissolution events contribute to the cumulative function, R, and each will have an associated activation energy nE_b (BKL algorithm step 2) that will vary depending on their local neighbourhood. For both adatom diffusion and dissolution events, the governing activation energy will be the one associated with the particular event that is carried out (BKL algorithm step 4). Fig. 3a and b shows the activation energies governing adatom diffusion and dissolution steps for the first 2.5 s and 300 s of simulated leaching of $NiAl_3$. Outputted at regular intervals, each point is the mean value of activation energy for either diffusion or dissolution processes occurring over the previous 100 sampling steps. From this figure, it is clear that the activation energy governing diffusion is several times smaller than that governing dissolution.

From Fig. 3b, the activation energy for dissolution generally lies in a range of 100–120 kJ mol^{-1}; although once the bulk of Al has been removed, the computed values become more scattered as dissolution events become more infrequent, an effect which is exaggerated by the relatively small number of atoms in the model. Fig. 3a shows the activation energy governing dissolution early on in the leaching simulation is as low as 65 kJ mol^{-1}, and for the first 2 s, a fairly steady 100 kJ mol^{-1} prevails. This is consistent with experimentally measured activation energies ranging from 42

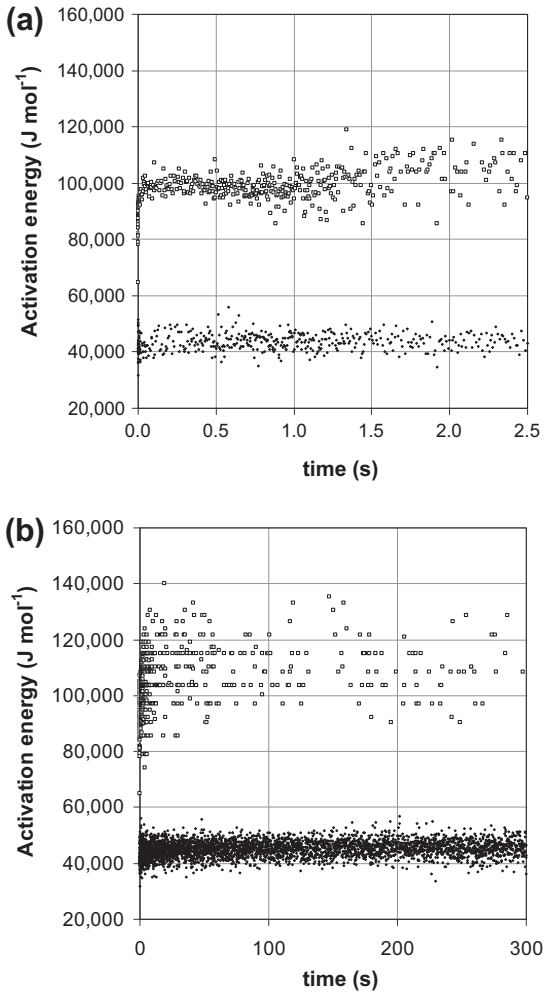

Fig. 3. Calculated activation energies for adatom diffusion (lower series) and Al dissolution (upper series) during leaching of $NiAl_3$ (dissolution attempt frequency $10^{17}\ s^{-1}$ and diffusion attempt frequency $10^{13}\ s^{-1}$) for (a) the first 2.5 s of simulation and (b) the first 300 s of simulation.

to 103 kJ mol^{-1} for a range of binary Ni_xAl_y alloys, where an increase in activation energy with increasing Ni content was observed [45]. Referring to Fig. 3b, it is noted that the activation energies for dissociation are higher than those for diffusion simply because the apparent pre-exponential factor for dissociation is much higher than the pre-exponential factor for diffusion. In reality, the difference is also related to the difference in the dynamics.

For adatom diffusion, the governing activation energy is more tightly centred on a value of 45 kJ mol^{-1}. Antczak and Ehrlich [46] provide a comprehensive review of published surface diffusion data, derived from both experimental and numerical methods for a variety of metals. For the case of Ni on (1 0 0), Ni surface diffusion values reported range from 45 to 125 kJ mol^{-1}. The value calculated from the kMC model is at the lower end of this range, but in our model, coarsening occurs mainly by edge/step diffusion that will be easier compared to diffusion across a 2D plane. Thus for adatom diffusion and Al dissolution, the governing activation energies in the model are reasonable when compared to published data.

2.6. Metropolis Monte Carlo model

The advantage of the kMC approach is its ability to simulate leaching over times comparable to industrial practice. However, in the kMC model, only dissolution and surface diffusion occur that permits considerably less computational effort because only surface atoms are considered in the simulation. However, it does represent a significant computational simplification because diffusion of Al atoms from the interior to the surface is ignored. To provide some justification for this approach, it is known that Al dissolution occurs rapidly, and coarsening of the structure by surface diffusion will be dominated by edge diffusion, both processes occurring much faster than diffusion in the interior. The coarsening of the structure itself will also reveal unleached Al atoms at the surface where they can dissolve.

To overcome the limitations of the kMC model and to investigate possible segregation effects where atoms move between internal and surface sites, a Metropolis Monte Carlo model, described below, is employed. In contrast to the kMC model, the Metropolis model includes anisotropy in the pair–pair interactions but makes the assumption that coarsening of the structure has become negligibly slow.

In order to address the experimental observations that leached Raney-Ni catalytic powders composed of <10% aluminium and can possess 30–50% metallic aluminium at the surface, a Metropolis Monte Carlo (MMC) modelling approach has been adopted. The MMC algorithm differs from the kinetic Monte Carlo method (kMC) in that it attempts to determine the minimum energy for a system, but without reference to time. The kMC technique has been used to simulate the time evolution of nano-porous structures during leaching. In contrast, the MMC technique is used here to determine the lowest energy configuration for these computed structures in terms of optimum interatomic spacings and distribution of atomic species.

The general MMC algorithm is described widely in the literature, e.g., [47]. Here, it is used in the isothermal-isobaric ensemble. The number of atoms, N, temperature (300 K) and pressure are fixed. The number of each kind of atom (Ni or Al) is also fixed. Two types of trial are performed.

(1) Random displacement of each atom in the computational domain from its current position. The magnitude of this displacement is of the order 0.003 Å. Once each atom has been displaced; the decision on acceptance of the new configuration is based on the standard Metropolis method:

$$\mathrm{Pr} = \exp\left(\frac{-\Delta U}{kT}\right) \tag{4}$$

where kT is the Boltzmann factor and ΔU is the potential energy difference. If the probability Pr is greater than unity, the new configuration is accepted. Otherwise it is still accepted with a probability of Pr.

(2) An atom is exchanged with another atom selected at random. The decision on acceptance of the change is also according to Eq. (4) above.

After all atoms in the simulation have undergone several of these steps, the lattice parameter of one box direction, [0 0 1], [0 1 0] or [1 0 0], is selected at random and altered. Random changes in lattice parameter of up to 1 Å are used. The probability, Pr, of acceptance of such an alteration is given by:

$$\mathrm{Pr} = \exp\left(\frac{-(\Delta U + P\Delta V - NkT\ln V)}{kT}\right) \tag{5}$$

Here, V is the volume of the box, and P is pressure (assumed to be zero). This acceptance criterion is based on the standard Metropolis method in Eq. (4) [48].

These trials are repeated until the system effectively reaches a steady state where the cohesive energy per atom and the predicted lattice parameters converge and the surface concentration of Al do not change with further trials. While several data sets have been

made available to model NiAl alloys, we choose the tight-binding (TB) second-moment approximation (SMA) approach adopted by Papanicolaou et al. [49]. This TB-SMA approach defines the total energy of the system (U in Eq. (4)) as

$$U = -\sum_{i=1}^{N}\left(\sum_{j\neq i} A_{\alpha\beta}\exp\left[-p_{\alpha\beta}\left(\frac{r_{ij}}{r_0^{\alpha\beta}}-1\right)\right] - \left\{\sum_{j\neq i}\xi_{\alpha\beta}^2\exp\left[-2q_{\alpha\beta}\left(\frac{r_{ij}}{r_0^{\alpha\beta}}-1\right)\right]\right\}^{1/2}\right) \quad (6)$$

Here, the first term is a pair-potential repulsive term, and the second term corresponds to the band-structure term. N is the total number of atoms, r_{ij} is the distance between atoms i and j of the species α and β, respectively (α and β stand for Al or Ni) and the sum j is extended up to fifth neighbours. Numerical values of the constants A, ξ, p, q and r_0 are given in [49]. MMC simulations of this type have been carried out in the past to investigate the surface configurations of isolated nano-clusters of Ni_xAl_y alloys, e.g., [48]. Using this data set, the cohesive energy per atom converges to −4.176 eV the predicted lattice parameters converge to 0.344 nm.

In summary, a kMC model is used to generate a nano-porous structure that aims to be representative of real as-leached spongy nickel. The predicted 3D arrangement is then used as a reference structure upon which different proportions of Ni and Al atoms can be placed. While maintaining the numbers of Al and Ni atoms constant, the MMC algorithm repeatedly swaps Al and Ni atoms whilst also adjusting the overall lattice parameters to compute the lowest energy configuration for the given atomic arrangement and relative proportions of Al and Ni atoms. No further diffusion or leaching occurs during the MMC simulation. The MMC model is thus used in a similar manner to published work on isolated spheroidal nano-clusters of different compositions [48]. The important difference here is that the simulation is carried out on a non-spheroidal cluster. The effectiveness of using this two-stage approach is discussed later. Simulations were performed on standard 2.66 GHz PCs. A complete kMC/MMC simulation on a grid with 200^3 atoms would take approximately 500 h. The MMC simulation presented here required 3×10^7 iterations (~1000 per atom) for convergence, where each Monte Carlo step is equivalent to a sampled event. This is extended to 8.6×10^7 in the case of the kMC model described in this paper, which corresponds to approximately 2500 Monte Carlo steps per atom.

3. Experimental

3.1. Preparation of the catalysts

Alloy atomised powders Ni–Al 68.5 at.% were received from CERAM. The atomisation process used to prepare the starting alloy is described elsewhere [4]. Starting powders were treated with an excess of an aqueous 20 wt.% sodium hydroxide solution. This excess of concentrated sodium hydroxide (more than 10 wt.%) is required to avoid the precipitation of Bayerite ($Al_2O_3{\cdot}H_2O$), which can block the pores of the catalyst by covering the nickel surface [2]. The powder was slowly introduced into the sodium hydroxide solution at 50 °C. Due to the exothermic reaction, the temperature increased quickly to around 80 °C, which was kept constant during the reaction. The sodium hydroxide was removed after the desired reaction time, and the resulting powders were washed in distilled water. The leaching process is complete after 3 h of reaction. In order to study surface composition as function of the leaching time, the leaching process was interrupted after 30 min and 90 min by washing the powder with distilled water until no more hydrogen gas evolves. To avoid exposure to air, the different samples were kept immersed in water prior to the characterisation experiments. In order to study the influence of particle size of the initial atomised alloy on surface composition, various ranges of grain sizes were used.

3.2. Inductively coupled plasma optical emission spectroscopy

Elemental analysis of the various catalyst was performed by ICP-OES (inductively coupled plasma optical emission spectroscopy) using a Varian Vista-MPX. For that purpose, 0.05 g of powder was dissolved in a 6% solution of nitric acid and the solution was diluted by a factor of 1000 with distilled water before measurements.

3.3. X-ray photoelectron spectroscopy

The Raney-type Ni catalyst samples were dried under a protective atmosphere. The XPS analysis was performed with an ESCALAB MKII (VG scientific) system equipped with a dual anode X-ray source (Mg/Al) and a spherical analyzer. The instrument was set at a constant analyzer pass energy of 50 eV, and Al $K\alpha_{1,2}$ radiation with a photon energy of 1486.6 eV was used for excitation. The electrons emitted by the sample were detected at an angle of 45° with respect to the sample surface. Spectra were recorded of the Ni *2p*, Ni *3s*, Al *2p*, Al *2s*, photoelectron lines with a step size of 0.1 eV. The Ni $2p_{3/2}$ binding energy of metallic Ni (852.80 eV) was used as an internal reference. The carbon C *1s* peak (285 eV) was used as internal reference in order to correct for the shift in binding energy due to charging of the sample. The surface composition of the catalyst was determined from the integrated intensity of the Ni *3s*, Al *2s* photoelectron lines by adopting the elemental sensitivity factors [50,51]. CasaXPS software was used to deconvolute the recorded spectra.

3.4. BET measurements

BET surface areas of the catalysts were measured by N_2 physisorption at −196 °C with an automatic Qsurf M1 analyzer (Thermo Finnigan). A special cell was designed to dry the Raney-type nickel catalysts by evacuating the liquid. Prior to each measurement, the catalyst was degassed for 3 h in helium at 150 °C to remove the adsorbed impurities. For each measurement, at least three points were taken to calculate the total surface area of the samples.

4. Results and discussion

4.1. XPS qualitative analysis

Fig. 4 shows the Ni 2*p* region of Raney-type nickel catalyst prepared from Ceram Ni–Al 75 at.% 106–150 μm. This spectrum is representative of all various homemade catalysts prepared. After correcting for sample charging, the position of the Ni $2p_{3/2}$ emission line was observed at 852.8 eV, corresponding to Ni^0. The Ni^0 $2p_{1/2}$ emission line was observed at 870 eV, which is in good agreement with the doublet separation of 17.2 eV reported in the literature [50]. The peak at 858 eV is attributed to the typical metallic Ni satellite. Due to the presence of this satellite, it is hard to conclude on the complete absence of nickel oxide that should appear between 854 and 855 eV, but its presence would be not be significant.

The spectra comprising the Al 2*s* and the Ni 3*s* area are given in Fig. 5. In this figure, the catalyst surface was also analysed at various leaching times (Fig. 5c) and various particle sizes of the starting alloy (Fig. 5a). A broad band at approximately 120 eV can be seen, which indicates the presence of Al^{3+} [50] for shorter leaching time (30 min and 90 min). The emission line measured at 117.6 eV

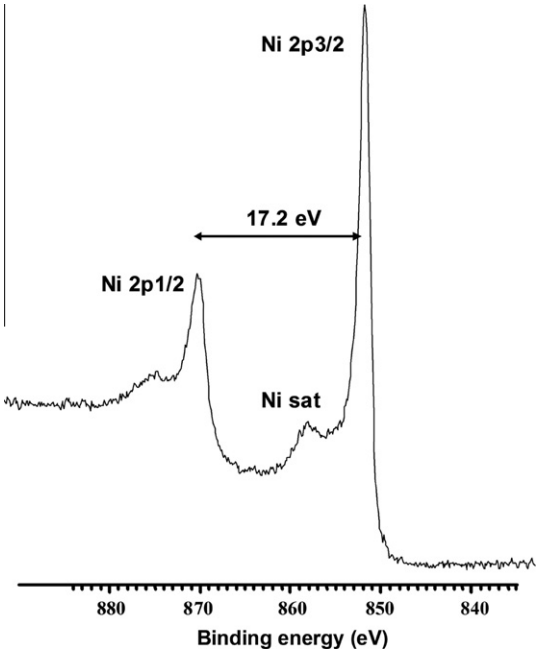

Fig. 4. Ni *2p* area of Raney-type nickel catalysts: Ni in metallic state.

is attributed to metallic aluminium [50]. After leaching times of 30 min and 90 min, a significant amount aluminium is still present at the surface. This can be attributed to the fact that the leaching process is not complete and that dissolved aluminium (Al^{3+}) is still present in the catalysts. After 180 min of leaching, mainly metallic aluminium is present at the surface. Fig. 5b illustrates the shift from ionic aluminium at short leaching times to mainly metallic aluminium when leaching is considered to be complete. In Fig. 5a, no significant differences were observed in XPS spectrum for different particle sizes of the starting atomised powder.

In summary, the following information was obtained from XPS:

- Only metallic nickel is present at the surface.
- The amount of aluminium at the surface decreases with increasing leaching time.
- After a short leaching time, aluminium is present at the surface as an oxide or hydroxide. In contrast, after a longer leaching time, mainly metallic aluminium is present.

Table 1
Surface composition of Raney-type nickel catalysts prepared from atomised powders (CERAM) after various leaching times and using different initial particle sizes.

Particle size of starting alloy (Ni–Al 68.5 at.%) (μm)	Leaching time (min)	At.% Ni	At.% Al
75–106	30	25	75
106–150	30	22	78
150–212	30	21	79
75–106	90	27	73
106–150	90	28	72
150–212	90	30	70
75–106	180	52	48
106–150	180	54	46
150–212	180	54	46

4.2. XPS quantitative analysis, bulk analysis and BET measurements

The Ni/Al ratio at the surface can be determined from the peak intensity ratios by using the proper sensitivity factors [50,51]. Results are reported in Table 1. When the leaching process is not complete (30 min and 90 min of leaching time), 70–80% of remaining aluminium is present at the surface. At these early times, the leaching process has not permitted full dissolution of the aluminium that is still present at the surface as aluminium oxide or hydroxide. The remarkable result is the large amount of aluminium present at the surface when the leaching process is complete (180 min): around 50% of aluminium is still present at the near surface. This contrasts with simulation results that typically give a maximum of 33 at.% of aluminium remaining at the surface after leaching. However, it is known that the Ni_2Al_3 phase present in the starting material does not leach properly and is still present in the final catalyst [20,52,53]. Raney-type nickel catalyst is commonly described as an agglomerate of nano-crystallites of nickel, the size of those nano-particles being ideally less than 5 nm. X-ray photoelectron spectroscopy is a near-surface technique; up to 10–15 layers in depth contribute to the signals, corresponding to a few nanometres, generally less than the predicted characteristic pore sizes. Hence, Ni_2Al_3 that remains in the catalyst might contribute to the XPS signals, a factor that is not simulated by our models. To investigate this apparent discrepancy further, an extra

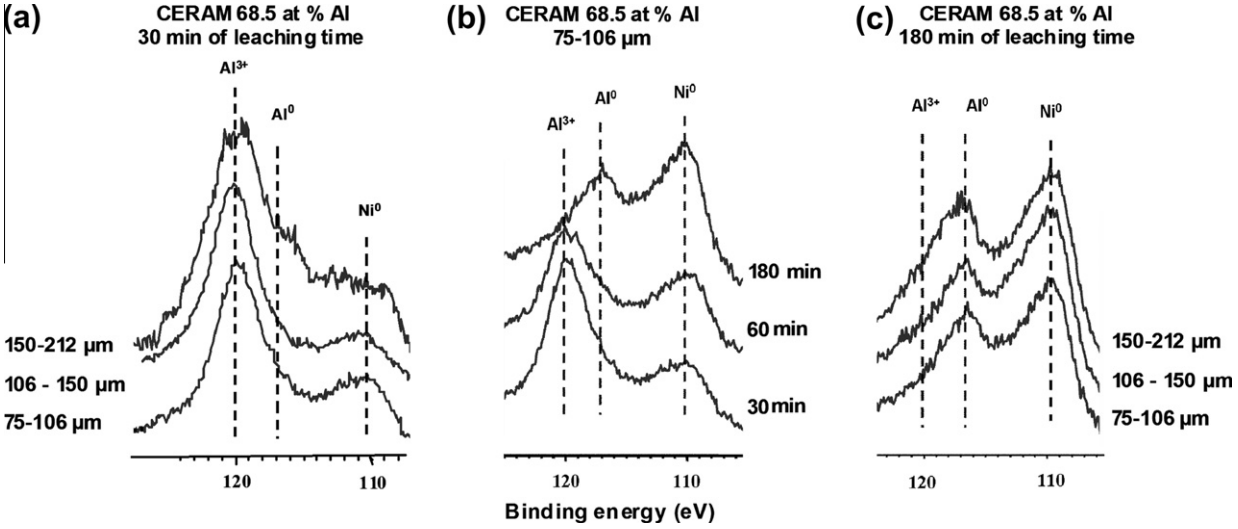

Fig. 5. Ni *3s* and Al *2s* area: various particle size after 30 min of leaching (a) and 180 min of leaching (c) and from 30 to 180 min of leaching with fixed particle size (b).

Table 2
Measured bulk (ICP OES) and surface (XPS) Ni and Al concentrations and measured (BET) and predicted surface areas for 68.5 at.% and 82.5 at.% precursor materials.

Catalysts	Ni (at.%) ICP OES	Al (at.%) ICP OES	Ni (at.%) XPS	Al (at.%) XPS	BET measured ($m^2\ g^{-1}$)	Surface area predicted ($m^2\ g^{-1}$)
Ni–Al 68.5 at.% 106–150 μm	83 ± 1	17 ± 1	54 ± 1	46 ± 1	43 ± 2	43.95
Ni–Al 82.5 at.% 106–150 μm	95 ± 1	5 ± 1	68 ± 1	32 ± 1	48 ± 2	49.90

experiment has been carried out. Raney-type nickel catalyst was prepared from atomisation powder with a composition of Ni–Al 82.5 at.% 106–150 μm. According to the phase diagram, there should be no Ni_2Al_3 present in this alloy. This was confirmed by neutron diffraction and X-ray tomography [29]. After proper leaching (i.e., 180 min), the near-surface composition (XPS) is 32 at.% of Al. The results are reported in Table 2.

It is interesting to note that the remaining aluminium in the bulk (ICP-OES) is significantly larger when Ni_2Al_3 is present in the starting alloy (Ni–Al 68.5 at.% 106–150 μm). This tends to confirm the fact that after leaching, two different types of aluminium are present in our system: aluminium from residual Ni_2Al_3 (not simulated) and aluminium that actually remains at the surface in a metallic state even after leaching.

4.3. Simulation results

Fig. 6 shows the very early stages of leaching and is very similar in appearance to published 'spongy Nickel' structures leached for only a few seconds [28]. Fig. 7 shows the final structure predicted by the kMC and MMC models for a structure that was initially wholly $NiAl_3$ phase that also closely resembles published TEM images of leached Raney-Ni material [28] leached for much longer times. (The ability of the model to produce leached structures similar to observed leached $NiAl_3$ and Ni_2Al_3 material has previously been shown [24].) This model was run in a cubic domain with an edge length containing 200 atoms. To estimate surface area, we use the GRID/OEPP (one element per point) method [54–56]. The structure is considered as a system of overlapping spheres surrounded by a rectangular box. An orthogonal mesh with individual element edge lengths $\boldsymbol{a}$ is then constructed cutting the three edges in *NX*, *NY* and *NZ* points, i.e., the box contains $NX \times NY \times NZ$ points.

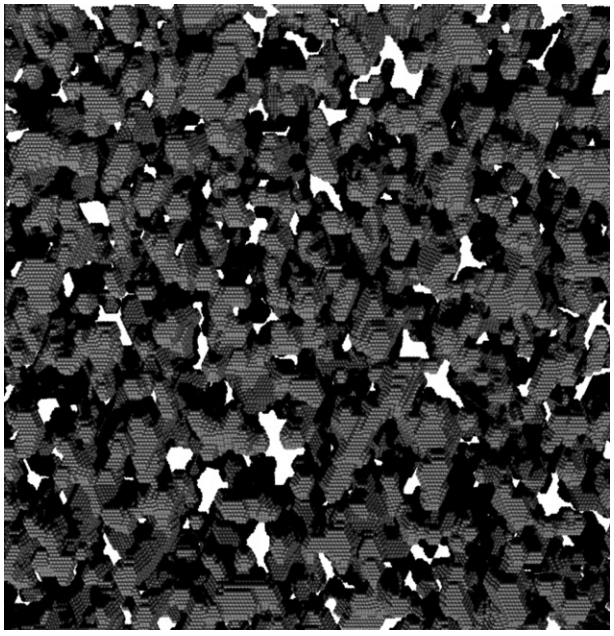

Fig. 6. Predicted nano-porous structure in the very early stages of simulated leaching (<30 s) of an initial $NiAl_3$ structure using a kinetic Monte Carlo model.

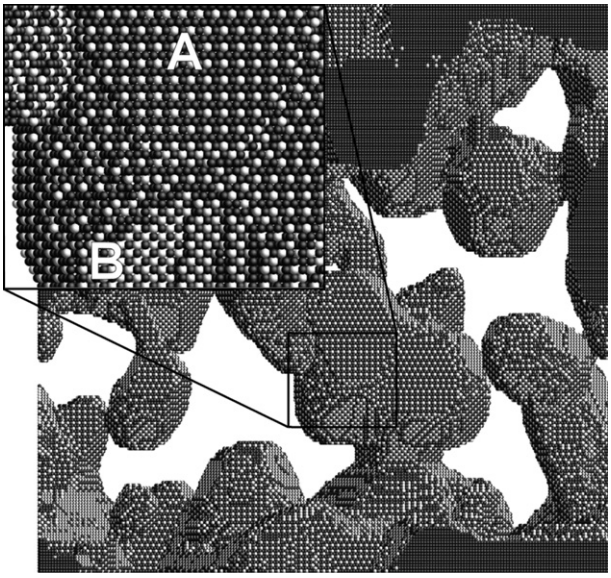

Fig. 7. 3D predicted nano-porous structure of leached $NiAl_3$ precursor material. The box at the top left shows a magnified view. Region A is an exposed (1 1 1) plane and just to the right of B is an exposed (1 0 0) plane. Dark atoms are Ni, and light atoms are Al. Edge length of the larger box is 50 nm. Calculated surface area is 49.9 $m^2\ g^{-1}$, the bulk Al composition is 5 at.% and the mean surface Al composition is 28.9 at.%.

Each point in the box is examined sequentially. Points at the surface contribute a value of $\boldsymbol{a}^2$ to the total surface area. The value of $\boldsymbol{a}$ was set equal to the Ni lattice parameter, 0.352 nm.

In Fig. 6, the calculated surface area is 49.9 $m^2\ g^{-1}$, the bulk Al composition is 5 at.% and the surface Al composition is 28.9 at.% (close to the 32% Al value for the Ni–Al 82.5 at.% precursor material with no Ni_2Al_3 phase present prior to leaching). The same simulation for a mesh that is initially constructed as Ni_2Al_3 phase yields a computed surface area of 33.0 $m^2\ g^{-1}$. In the model, these surface areas are calculated from a small region of nano-porous material.

In reality, the leached catalyst particles will also possess a micro-scale porous structure [29]; however, the contribution of this micro-scale porosity to the overall value is not included in the present model. The presence of mainly metallic aluminium at the surface after complete leaching is in good agreement with the MMC simulations that suggest that virtually no Al–Al bonds are present in the system (Fig. 8).

Prior to leaching, each of the catalyst materials in Table 2 consists of different proportions of Ni_2Al_3, $NiAl_3$ and Al-eutectic phases. These proportions for the 68.5 at.% Al material are shown in Table 3. The 82.5 at.% Al material effectively contains only $NiAl_3$ and eutectic (i.e., <5 at.% Ni_2Al_3). Full details of precursor and leached material, including 3D tomography images, are given in [29]. Assuming that the effectively pure Al phase is completely removed during the initial stages of leaching then the final surface area of the leached material could be estimated via a simple weighted average of the computed surface areas associated with each phase after leaching. These predicted surface areas are also shown in Table 2, and considering the very small region of material simulated in the model, these are close to the measured BET data. This lends confidence to the idea that the predicted nano-porous structure in Fig. 7 is representative of as-leached spongy nickel.

The final predicted densities for leached $NiAl_3$ and leached Ni_2Al_3 phases are 1.53 and 2.44 g/cm^3, respectively, although only very small regions of material have been simulated. Larger scale micro-porosity coupled with the presence of unleached material in whole particles of catalyst is not included.

As an aside, the measured value [50] of surface aluminium content for an exposed (1 1 1) plane is 25 at.% ($Ni_{90}Al_{10}$ at 1100 K). A theoretical maximum of surface aluminium content for an exposed (1 0 0) plane, precluding any Al–Al bonds, is 50 at.%. Since a structure predominantly comprising exposed (1 1 1) and (1 0 0) planes is predicted by the model, it might therefore be expected that as-leached Raney-Ni powders with residual Al would possess surface concentrations of Al in the range 25–50 at.%, which is routinely observed in experimental measurements.

Finally, despite their limitations, these relatively simple models of a complex process have shown some promise in starting to understand the structural evolution of Raney-Ni catalyst material during leaching. As is often the case, the interplay between experimentalists and modellers is mutually beneficial. However, it is still the case that there are many structural and morphological features of these multiscale-porous structures that are not fully quantified and the role of both nanometric and micrometric structural features during catalysis are not fully understood. Were they to become fully validated, numerical predictions regarding surface areas, Al surface segregation and details of surface coordination numbers could provide the basis for further modelling approaches, e.g., density functional theory, in an attempt to start predicting catalytic performance. However, the variety of different possible chemical reactions, the role of small dopant additions, etc. all present significant extra challenges.

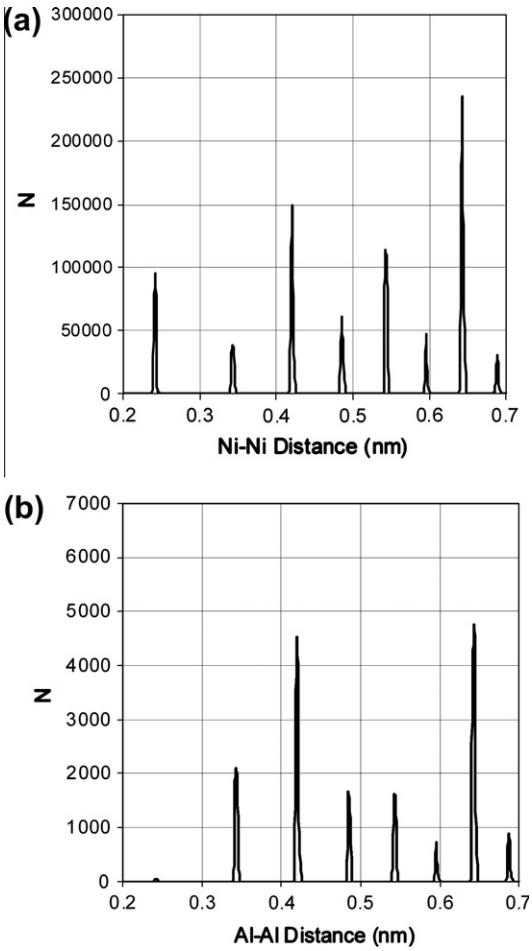

Fig. 8. Central distance frequency distributions for the surfaces in Fig. 7 for (a) Ni–Ni distances and (b) Al–Al distances at 300 K showing an almost complete lack of Al–Al bonds at the surface.

Table 3
Measured phase proportions of catalyst prior to leaching.

Catalyst	$NiAl_3$ (%)	Ni_2Al_3 (%)	Al (%)
Ni–Al 68.5 at.% 106–150 μm	33.46	61.58	4.96

5. Conclusions

Firstly, a lattice kinetic Monte Carlo model has been used successfully to predict the surface areas measured for leached Raney-Ni catalyst material produced from spray-atomised precursor material using two different Ni_xAl_y alloys. The activation energy governing diffusion is found to be lower than that governing dissolution, and both values are at least consistent with published data. Secondly, taking a pragmatic approach, an off-lattice Metropolis Monte Carlo model has subsequently been used to investigate segregation of residual Al in the simulated leached nano-porous structure. Using this two step approach reduces computational effort considerably but represents a numerical simplification because in the kMC model, diffusion of Al to the surface is not included, and in the MMC model, further coarsening is not considered. However, despite these limitations and the uncertainty associated with the model parameters, a good match to experimental results has been achieved.

The presence of residual unleached Ni_2Al_3 phase (which is not accounted for in the model) has been demonstrated to influence the amount of surface Al measured via XPS in such leached catalyst material. This effect was removed by using a precursor alloy that does not contain the Ni_2Al_3 phase [29]. Even though this alloy only contained 5 at.% Al by volume after leaching, the model predicts the surface Al composition is 28.9 at.% (close to the measured 32% Al value). Also, for two alloys of different initial composition, the model correctly predicts the observed difference in final catalyst surface topology. Finally, the model also predicts a virtual lack of Al–Al bonds at the surface, also in agreement with previous published results.

Acknowledgments

The authors would like to acknowledge the helpful inputs of the reviewers. This work was carried out as part of the EU IMPRESS project (Intermetallic Materials Processing in Relation to Earth and Space Solidification) [57]. The authors would like to express their gratitude for financial support from IMPRESS Integrated Project (Contract NMP3-CT-2004-500635) co-funded by the European Commission in the Sixth Framework Programme and the European Space Agency.

References

[1] M. Raney, US patent 1,563,787, 1925.
[2] P. Fouilloux, G.A. Martin, A.J. Renouprez, B. Moraweck, B. Imelik, M. Prettre, J. Catal. 25 (1972) 212.
[3] A. J Smith, D.L. Trimm, Annu. Rev. Mater. Res. 35 (2005) 127.
[4] F. Devred, A.H. Gieske, N. Adkins, U. Dahlborg, C.M. Bao, M. Calvo-Dahlborg, J.W. Bakker, B.E. Nieuwenhuys, Appl. Catal. A: Gen. 356 (2009) 154.
[5] A.B. Fasman, V.F. Timofeeva, V.N. Rechkin, Y.F. Klyuchnikov, Kyn. Khem. 13 (1971) 1513.
[6] J. Freel, W.J.M. Pieters, R.B. Anderson, J. Catal. 14 (1969) 247.
[7] S. Sane, J.M. Bonnier, J.P. Damon, J. Masson, Appl. Catal. 9 (1984) 69.
[8] M.S. Wainwright, in: G. Ertl, H. Knozinger, J. Weitkamp (Eds.), Handbook of Heterogeneous Catalysis, vol. 1, VCH Publ., New York, 1997, pp. 64. ISBN:3-527-29212-8.
[9] R. Holm, S. Storp, J. Electron Spectrosc. Related Phenom. 8 (1976) 139.

[10] S. Hamar-Thibault, J. Gros, J.C. Joud, J. Masson, J.P. Damon, J.M. Bonnier, in: V.G. Poncelet, P.A. Jacobs, P. Grange, B. Delmon (Eds.), Preparation of Catalysts, V-Scientific Bases for the Preparation of Heterogeneous Catalysts, Elsevier Science Publishers B.V., Amsterdam, 1991, pp. 601–610.
[11] F. Delannay, J.P. Damon, J. Masson, B. Delmon, Appl. Catal. 4 (1982) 169–180.
[12] S. Hamar-Thibault, J. Masson, J. Chim. Phys. 88 (1991) 219–232.
[13] J.M. Bonnier, J.P. Damon, B. Delmon, B. Doumian, J. Masson, J. Chim. Phys. 84 (1987) 889–894.
[14] H. Hu, F. Xie, Y. Pei, M. Qiao, S. Yan, H . He, K. Fan, H. Li, B. Zong, X. Zhang, J. Catal. 237 (2006) 143–151.
[15] S.D. Mikhailenko, A.B. Fasman, N.A. Maksimova, E.V. Leongard, E.S. Shpiro, G.V. Antoshin, Appl. Catal. 12 (1984) 141–150.
[16] S.D. Mikhailenko, T.A. Khodareva, E.V. Leongard, A.I. Lyashenko, A.B. Fasman, J. Catal. 141 (1993) 688–699.
[17] U. Birkenstock, R. Holm, B. Reinfandt, S. Storp, J. Catal. 93 (1985) 55–67.
[18] Y. Okamoto, Y. Nitta, I. Imanata, S. Teranishi, JCS Faraday I 76 (1980) 998–1007.
[19] N. Mahata, A.F. Cunha, J.J.M. Ó rfao, J.L. Figueiredo, Appl. Catal. A: Gen. 351 (2008) 204.
[20] H. Lei, Z. Song, D. Tan, X. Bao, X. Mu, B. Zong, E. Min, Appl. Catal. A: Gen. 214 (2001) 69.
[21] C.C. Battaile, Comput. Methods Appl. Mech. Eng. 197 (2008) 3386–3398.
[22] D.N. Theodorou, Ind. Eng. Chem. Res. 49 (2010) 3047–3058.
[23] N.C. Barnard, S.G.R. Brown, in: V.G. DeGiorgi, C.A. Brebbia, R.A. Adey (Eds.), Simulation of Electrochemical Process II, WIT Press, Southampton, UK, 2007, pp. 53–62. ISBN:978-1-84564-071-2.
[24] N.C. Barnard, S.G.R. Brown, F. Devred, B.E. Nieuwenhuys, Electrochemical process simulation III, in: C.A. Brebbia, R.A. Adey (Eds.), Proceedings of the 3rd International Conference on Simulation of Electrochemical Processes, WIT Press, Southampton, UK, 2009, pp. 151–161. ISBN:978-1-84564-192-4.
[25] J. Erlebacher, M.J. Aziz, A. Karma, N. Dimitrov, K. Sieradzki, Nature 410 (2001) 450–453.
[26] W. Schmickler, Electrochim. Acta 41 (1996) 2329–2338.
[27] R. Wang, H. Chen, Z. Lu, S. Qiu, T. Ko, J. Mater. Sci. 43 (2008) 5712–5719.
[28] F. Devred, B.W. Hoffer, W.G. Sloof, P.J. Kooyman, A.D. van Langeveld, H.W. Zandbergen, Appl. Catal. A: Gen. 244 (2003).
[29] F. Devred, G. Rheinhart, G.N. Iles, B. van der Klugt, N.J. Adkins, J.W. Bakker, B.E. Nieuwenhuys, Catal. Today, in press. doi:10.1016/j.cattod.2010.01.054.
[30] J. Erlebacher, J. Electrochem. Soc. 151 (2004) C614–C626.
[31] G.S. Bales, D.C. Chrzan, Phys. Rev. B 50 (1994) 6057–6067.
[32] J.D. Erlebacher, M.J. Aziz, Surf. Sci. 374 (1997) 427–442.
[33] E. Pichardo-Pedrero, M. Giesen, Electrochim. Acta 52 (2007) 5659–5668.
[34] E. Pichardo-Pedrero, G.L. Beltramo, M. Giesen, Appl. Phys. A 87 (2007) 461–467.
[35] J. Ikonomov, K. Starbova, H. Ibach, M. Giesen, Phys. Rev. B 75 (2007) 245411.
[36] K. Pöttinga, N.B. Luquea, P.M. Quainoa, H. Ibach, W. Schmickler, Electrochim. Acta 54 (2009) 4494–4500.
[37] H.J.W. Zandvliet, Surf. Sci. 604 (2010) 1261–1264.
[38] J. Mei, B.R. Cooper, S.P. Lim, Phys. Rev. B 54 (1996) 178–183.
[39] M.I. Baskes, C.F. Melius, Phys. Rev. B 20 (1979) 3197–3204.
[40] K.W. Jacobsen, J.K. Norskov, M.J. Puska, Phys. Rev. B 35 (1987) 7423–7442.
[41] Y. Mishin, M.J. Mehl, D.A. Papaconstantopoulos, Phys. Rev. B 65 (2002) 114–224.
[42] M.W. Finnis, J.E. Sinclair, Philos. Mag. A 50 (1984) 45–55.
[43] W.R.L. Lambrecht, Phys. Rev. B 34 (1986) 7421–7424.
[44] V.P. Zhdanov, Elementary Physicochemical Processes on Solid Surfaces, Plenum, New York, 1991.
[45] H. Hu, M. Qiao, Y. Pei, K. Fan, H. Li, B. Zong, X. Zhang, Appl. Catal. A: Gen. 252 (2003) 173–183.
[46] G. Antczak, G. Ehrlich, Surface Diffusion: Metals, Metals Atoms, and Clusters, Cambridge University Press, Cambridge, UK, 2010. ISBN:978-0-521-89983-3.
[47] M.P. Allen, D. Tildesley, Computer Simulation of Liquids, Clarendon, Oxford, 1987.
[48] E.E. Zhurkin, M. Hou, J. Phys. Condens. Matter 12 (2000) 6735–6754.
[49] N.I. Papanicolaou, H. Chamati, G.A. Evangelakis, D.A. Papaconstantopoulos, Comput. Mater. Sci. 27 (2003) 191–198.
[50] J.F. Moulder, W.F. Stickle, P.E. Sobol, K.D. Bomben, Handbook of X-ray Photoelectron Spectroscopy, Perkin-Elmer, Wellesley, 1992.
[51] ASTM E902-88, Surface and Interface Analysis 17 (1991) 4709.
[52] M.L. Bakker, D.J. Young, M.S. Wainwright, J. Mater. Sci. 23 (1988) 3921.
[53] R. Wang, Z. Lu, T. Ko, J. Mater. Sci. 36 (2001) 5649.
[54] A.Y. Meyer, Chem. Soc. Rev. 15 (1986) 449–474.
[55] A.Y. Meyer, J. Comp. Chem. 7 (1986) 144–152.
[56] A.Y. Meyer, J. Comput. Chem. 9 (1988) 18–24.
[57] D.J. Jarvis, D. Voss, Mater. Sci. Eng. A 413–414 (2005) 583–591.